

PEPSI Investigation, Retrieval, and Atlas of Numerous Giant Atmospheres (PIRANGA). I. The Ubiquity of Fe I Emission and Inversions in Ultra Hot Jupiter Atmospheres

SYDNEY PETZ,^{1,*} MARSHALL C. JOHNSON ,^{1,*} ANUSHA PAI ASNODKAR ,¹ ALISON DUCK ,¹ JI WANG (王吉) ,¹ ILYA ILYIN,² AND KLAUS G. STRASSMEIER^{2,3}

¹Department of Astronomy, The Ohio State University, 4055 McPherson Laboratory, 140 West 18th Ave., Columbus, OH 43210, USA

²Leibniz-Institute for Astrophysics Potsdam (AIP), An der Sternwarte 16, D-14482 Potsdam, Germany

³Institute of Physics & Astronomy, University of Potsdam, Karl-Liebknecht-Str. 24/25, D-14476 Potsdam, Germany

ABSTRACT

We present high-resolution optical emission spectroscopy observations of the ultra hot Jupiters (UHJs) TOI-1431 b and TOI-1518 b using the PEPSI spectrograph on the LBT. We detect emission lines from Fe I with a significance of 5.40σ and 7.85σ for TOI 1431 b and TOI-1518 b, respectively. We also detect Cr I emission from TOI-1431 b at 4.23σ . For TOI-1518 b, we tentatively detect Ni I, Fe II, and Mg I, as well as possibly CaH, at significance levels ranging from $3 - 4\sigma$. Detection of emission lines indicates that both planets possess temperature inversions in their atmospheres, providing further evidence of the ubiquity of stratospheres among UHJs. By analyzing the population of hot Jupiters, we compare models that predict the distribution of planets in the temperature-gravity space, and find a recent global circulation model suite from Roth et al. (2024) provides a reasonable match, if TiO is not included in the models. The ubiquity of strong Fe I emission lines among UHJs, together with the paucity of detections of TiO, suggest that atomic iron is the dominant optical opacity source in their atmospheres and can be responsible for the inversions.

Keywords: extrasolar gaseous giant planets; exoplanet atmospheres; exoplanet atmospheric structure; exoplanet atmospheric composition

1. INTRODUCTION

Ultra hot Jupiters (UHJs), short-period giant planets with dayside temperatures in excess of ~ 2200 K, are some of the most observationally accessible exoplanets. Their hot, bright daysides allow direct detection of light emitted from the planet with high-resolution spectroscopy (e.g., Pino et al. 2020; Yan et al. 2022; Brogi et al. 2023; Johnson et al. 2023; Petz et al. 2024). Many of these planets also reside around hot, bright, A- and early F-type stars, resulting in multiple targets around $V < 10$ stars for which the highest signal-to-noise ratio data can be obtained. Over the past few years, high-resolution emission spectroscopy has been published for nine bright UHJ targets. Those with optical spectra uniformly find strong Fe I emission lines indicating the presence of a temperature inversion in the atmosphere (e.g., Pino et al. 2020; Yan et al. 2020; Nugroho et al. 2020; Borsa et al. 2022; Scandariato et al. 2023; Hoeijmakers et al. 2024), while CO emission lines are seen in the

infrared (e.g., Yan et al. 2022, 2023). Other species are seen in both the optical and IR, including atomic metals like Fe II and Cr I and molecules like H₂O and OH (e.g., Scandariato et al. 2023; Brogi et al. 2023). In this paper, we add two more to the number of UHJs characterized with high-resolution emission spectroscopy: TOI-1431 b and TOI-1518 b, bringing the total sample size to eleven.

1.1. TOI-1431 b

TOI-1431 b (also known as MASCARA-5 b), is an exoplanet discovered by the *Transiting Exoplanet Survey Satellite* (*TESS*; Ricker et al. 2015) along with the Multi-site All-Sky CAmeRA (MASCARA; Talens et al. 2017) and confirmed to be a planet by Addison et al. (2021). Orbiting a bright ($V = 8.03$) Am star with an effective temperature of 7690 K at a period of 2.65 days, TOI-1431b has an equilibrium temperature of 2370 K. Due to the high temperatures of this UHJ, as well as its short orbital period, TOI-1431 b is a prime candidate for emission spectroscopy to investigate its atmospheric chemistry.

* These authors contributed equally to the work.

Stangret et al. (2021) used high resolution transmission spectroscopy to search for a variety of atomic and molecular species in the atmosphere of TOI-1431 b, but were unable to find any evidence of atmospheric features. They ascribed the lack of detections to this planet's relatively high surface gravity ($\log g = 3.54$ and consequent small atmospheric scale height. Stangret et al. (2021) also found that the orbit of TOI-1431 b is highly inclined with respect to the stellar rotation. We investigate the atmospheric chemistry of this planet using high resolution emission spectroscopy for the first time.

1.2. *TOI-1518 b*

TOI-1518 b is another ultra hot Jupiter discovered in *TESS* data by Cabot et al. (2021). It orbits a bright ($V = 8.95$), rapidly rotating F0 host star every 1.9 days, resulting in an equilibrium temperature of 2492 K. It is on a highly inclined, retrograde orbit, and nodal precession of the orbit was recently detected through photometric follow-up observations (Watanabe et al. 2024). Cabot et al. (2021) also detected absorption from both Fe I and Fe II during transit. TOI-1518 b was identified by Hord et al. (2023) as one of the five best UHJs for emission spectroscopy, but to our knowledge no observations of the dayside atmosphere have yet been published.

1.3. *Atmospheric Inversions*

Emission spectroscopy is sensitive to the pressure-temperature (P-T) profile in the photosphere of exoplanets. Decreasing temperature with altitude results in absorption lines in the spectrum, whereas an increasing temperature (a *temperature inversion*, also known as a stratosphere) results in emission lines. These can be detected with either high-resolution (e.g., Birkby et al. 2013; Brogi et al. 2023) or low-resolution space-based spectroscopy (e.g., Mansfield et al. 2018; Fu et al. 2022a).

An inversion requires the presence of a strong opacity source in the upper atmosphere, which absorbs incoming stellar radiation and heats the atmosphere. The most commonly invoked inversion agents for hot Jupiters are metal oxides like TiO and VO (e.g., Fortney et al. 2008). Observational searches for these species, however, have been controversial and had only limited success (e.g., Nugroho et al. 2017; Serindag et al. 2021; Prineth et al. 2022; Johnson et al. 2023). Many other species have been proposed as possible inversion agents, including other metal hydrides and oxides such as SiO, FeH, or CaH; atomic species such as Fe I or Mg I; or continuum opacity due to H⁻ (Lothringer et al. 2018; Gandhi & Madhusudhan 2019). Optical high-resolution spec-

troscopy is optimal for searching for these species, as they have many lines in this wavelength range.

Beatty et al. (2017a,b) found that two high-gravity objects lacked inversions (Kepler-13 Ab: $\log g = 4.0$, KELT-1 b: $\log g = 4.7$, even in the same equilibrium temperature range where lower-gravity objects have inverted atmospheres. They proposed that this is due to the presence of an atmospheric cold-trap related to the surface gravity, with higher-gravity objects possessing more efficient cold traps that would remove TiO and VO from their atmospheres and prevent the formation of a temperature inversion.

In this paper we search for the presence of atmospheric inversions in TOI-1431 b and TOI-1518 b, both of which have moderate surface gravity, using high-resolution spectroscopy (§2), as well as catalog the atomic and molecular species, including potential inversion agents, detectable in their atmospheres (see §3 for the methodology and §4 for the results). Subsequently (§5), we investigate the distribution of the presence of inversions (or the lack thereof) across the parameter space of hot Jupiters, and attempt to link this to the inversion agent(s).

2. OBSERVATIONS

We obtained time-series spectra of TOI-1431 and TOI-1518 for a duration of 4-7 hours per night using the Potsdam Échelle Polarimetric and Specrographic Instrument (PEPSI; Strassmeier et al. 2015) on the 2×8.4 m Large Binocular Telescope (LBT) located on Mt. Graham, Arizona, USA. We observed TOI-1431 on one night and TOI-1518 on two nights, the latter covering both pre- and post-secondary eclipse; we show the phase coverage in Fig. 1. We used the PEPSI 200 μ m fiber, giving a resolving power of $R = 130,000$, and used Cross Dispersers (CD) III and V, providing wavelength coverage of 4800-5441 Å and 6278-7419 Å in the blue and red channels, respectively. We used an exposure time of 250 seconds in each arm for each target. Further details of the observations are given in Table 1. The PEPSI CCDs were upgraded during the 2023 summer shutdown, and one of the LBT's two secondary mirrors was re-aluminized, resulting in comparable SNR (~ 200 -400) at a shorter exposure length (250 seconds) with respect to our previous observations of a brighter star (300 seconds for KELT-20, $V = 7.58$; Johnson et al. 2023; Petz et al. 2024). However, the 2024-01-14 UT TOI-1518 observations were of lower SNR than the 2023-11-06 UT dataset on the same planet due to poorer observing conditions (right panel of Fig. 1).

The environmental control system that typically keeps the pressure and temperature around the PEPSI optical

bench stable was disabled for the TOI-1431 observations due to a software fault. This resulted in some drift in the wavelength solution over the course of the observations; however, we were able to correct for this drift using the Fabry-Perot etalon simultaneous wavelength calibration system. There was no obvious effect on the recovery of the planetary signal from this drift, which amounted to less than 200 m s^{-1} , much smaller than the resolution of the instrument and the tens of km s^{-1} motion of the planetary lines over the course of the observations. We therefore do not expect any significant impact upon our results for TOI-1431 b.

The data were reduced using the SDS4PEPSI pipeline (Ilyin 2000; Strassmeier et al. 2018). The pipeline performs standard reduction steps, and produces an output 1-dimensional, wavelength-calibrated, continuum-normalized spectrum where the different orders and the traces from the two unit telescopes have been combined into a single spectrum. The pipeline also calculates the variance of each pixel, which we use to propagate uncertainties through the remainder of the analysis.

3. METHODOLOGY

Our methodology is largely the same as was used in Johnson et al. (2023) and Petz et al. (2024). In short, we first model out the telluric lines in the red-arm spectra using the MOLECFIT package (Smette et al. 2015; Kausch et al. 2015); although MOLECFIT performs well for correcting weak and moderately strong telluric lines, strong lines and bands are very difficult to correct and we exclude regions of the spectra strongly affected by tellurics from further analysis. We used a restricted wavelength range for the MOLECFIT models as compared to our previous work, choosing narrower ranges with fewer stellar lines: 6293-6298 Å, 6307-6314 Å, 6474-6483 Å, 6509-6517 Å, 7102-7110 Å, and 7358-7374 Å (all wavelengths given in the observatory rest frame). This was important for the relatively slowly rotating TOI-1431; with a $v \sin i$ of only 6 km s^{-1} (Addison et al. 2021), TOI-1431 is much more narrow-lined than either KELT-20 (Johnson et al. 2023; Petz et al. 2024) or TOI-1518. There is therefore a greater risk of MOLECFIT confusing stellar for telluric lines. We found that using these same wavelength ranges also resulted in a better fit (as measured by eye) to the telluric spectrum for TOI-1518, so we adopted them for both stars.

After telluric correction, we interpolate all of the time-series spectra from each PEPSI arm from a single night onto a common wavelength scale and create a median-combined spectrum, which is then removed from each

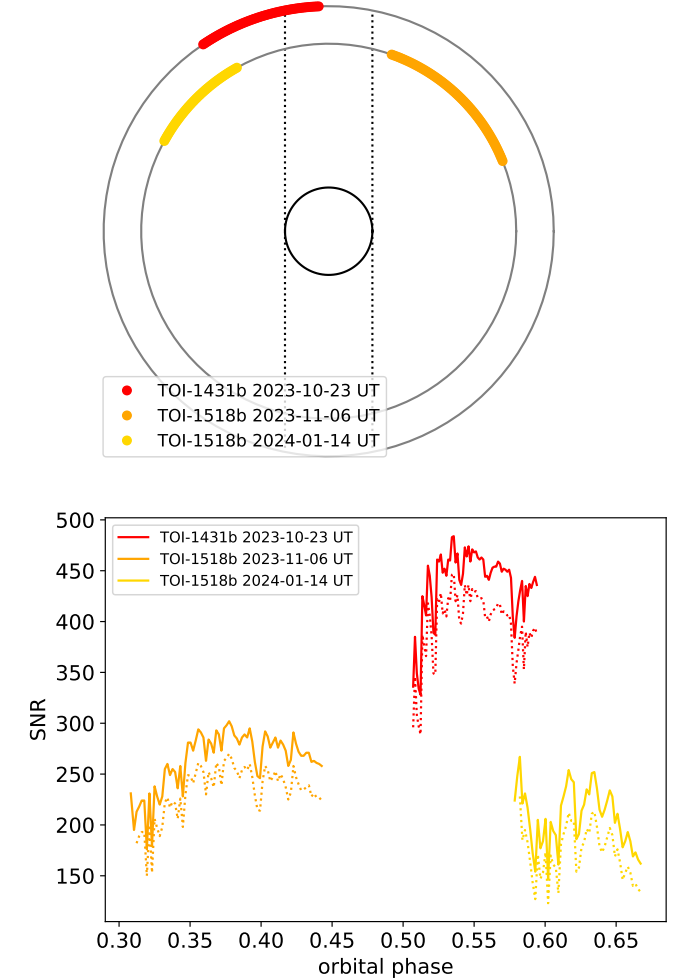


Figure 1. Left: Phase coverage of the observations used in this work. The solid inner circle shows the stellar surface, while the middle and outer circles show the orbits of TOI-1518 b and TOI-1431 b, respectively, to scale. The observer is off the bottom of the page, and the vertical dashed lines show the line of sight, such that transit occurs in the lower intersection of the dashed lines and planetary orbits, and the secondary eclipse in the upper intersection. The planets orbit counter-clockwise. The colored points show the portions of the orbit where we obtained data. Right: signal-to-noise ratio of our observations as a function of orbital phase. The PEPSI red and blue arms are shown as the solid and dotted lines, respectively. The SNR values shown are, for each spectrum, the 95th quantile per-pixel signal-to-noise ratios.

of the time series spectra. Next, we run the SYSREM algorithm (Tamuz et al. 2005) on the two-dimensional residuals in wavelength-time space in order to remove any imperfectly-removed telluric and stellar lines, and any instrumental systematics that might be present.

We then construct a model planetary emission spectrum using `petitRADTRANS` (Mollière et al. 2019). We

Table 1. Log of Observations

Target	Date (UT)	N_{spec}	Exp. Time (s)	Airmass Range	Phases Covered	SNR _{blue}	SNR _{red}
TOI-1431 b	2023-10-23	68	250	1.09 - 1.60	0.507 - 0.594	396	438
TOI-1518 b	2023-11-06	74*	250	1.21 - 1.43	0.311 - 0.445	232	264
TOI-1518 b	2024-01-14	50*	250	1.28 - 2.04	0.581 - 0.670	173	208

NOTE— N_{spec} is the number of spectra obtained on that night. Exp. time is the exposure time in seconds. SNR_{blue} and SNR_{red} are the nightly average of the 95th quantile per-pixel signal-to-noise ratios in the blue and red arms, respectively. *We excluded the first two blue-arm spectra from each TOI-1518 dataset, as well as the first red-arm spectrum from 2023 Nov. 6, due to solar contamination.

assume a pressure-temperature (P-T) profile of the form given by [Guillot \(2010\)](#), and include only a single line species in each model in addition to continuum opacity from H⁻, and collisionally-induced opacity from H₂-H₂ and H₂-He interactions. We adopted most planetary and stellar parameters from the discovery papers from the two systems, which are given in Table 2. We convolved each model spectrum with a model rotationally broadened line profile of the planet, as well as a model instrumental profile.

In order to assure that we correctly shift the data into the stellar rest frame for each target, we measured the stellar radial velocity in the PEPSI frame using the same methodology as in [Pai Asnodkar et al. \(2022\)](#) and [Petz et al. \(2024\)](#). Briefly, we use least squares deconvolution as implemented in [Kochukhov et al. \(2010\)](#) and [Wang et al. \(2017\)](#), with a **Spectroscopy Made Easy** ([Valenti & Piskunov 1996, 2012](#)) template spectrum, to extract the average stellar line profile from each time-series spectrum. We fit a rotationally broadened stellar line profile computed per [Gray \(2005\)](#) to the extracted line profiles, and use this to extract the stellar RVs. Finally, we fit a Keplerian model for a circular orbit to these RVs, including a zero-point offset which is the best-fit systemic RV in the PEPSI frame. We quote the resulting RV in Table 2.

Additionally, we utilize new ephemerides for both planets as the original discovery ephemerides are now several years old and additional *TESS* data are available. We fit the *TESS* photometry using **EXOFASTv2** ([Eastman et al. 2019](#)) in order to derive updated ephemerides. For both planets we were able to detect the secondary eclipses, providing additional leverage of the ephemeris and constraining the eccentricity (which is consistent with zero for both planets, so we assume circular orbits going forward). The updated ephemerides are listed in Table 2, and are part of a larger effort which will be presented in Duck et al. (in prep).

Next, we cross-correlated the model planetary spectrum with the time-series processed residual spectra, shifted each cross-correlation function (CCF) into the planetary rest frame assuming a range of planetary radial velocity (RV) semi-amplitude (K_P) values, and combined them to form a final CCF. We estimated the uncertainty in these maps from the standard deviation of regions at $|v_{\text{sys}}| > 100 \text{ km s}^{-1}$ from the expected planetary rest frame. We searched for peaks in this CCF map at the expected K_P , v_{sys} of the planet, and consider peaks with $> 4\sigma$ to be detections and those with $3 - 4\sigma$ to be tentative detections which will require more data to confirm. For TOI-1431, some of our spectra were taken during secondary eclipse. We excluded these spectra from the cross-correlation analysis, but they were used to compute the median spectrum and through the SYSREM analysis.

In order to set the P-T profile, we followed the methodology of [Johnson et al. \(2023\)](#) by conducting a simple, manual grid search in the parameters κ_{IR} (IR opacity), γ (ratio of optical to infrared opacity), T_{eq} , volume mixing ratio (VMR) of Fe I, and number of systematics removed with SYSREM, and adopted the parameters that resulted in the most significant detection of Fe I for each system. For each additional species, we vary its VMR in steps of 0.25 dex until we obtain the most significant detection. We emphasize that this is not an exhaustive search, and the resulting P-T profiles and VMR should be taken with caveats; in particular, we have not attempted to account or correct for the distortion of the planetary signal due to the SYSREM process ([Gibson et al. 2022](#)), nor to do a rigorous retrieval. We will pursue these analyses in a future paper. We show the best-fit P-T profiles in Fig. 2.

We searched for the following species: Fe I, Fe II, Ni I, Cr I, Ti I, Ti II, Mg I, Si I, Sc I, V I, Mn I, Sr I, Ca I, Ca II, TiO, VO, FeH, MgH, CaH, and CrH. We chose these species as they were found to be the most detectable in UHJs similar to TOI-1431 b and TOI-1518 b with

PEPSI by Petz et al. (2024), plus CrH, which was recently detected in WASP-31 b by Flagg et al. (2023). We used opacities from <http://kurucz.harvard.edu/> for the atomic species. For TiO, VO, and FeH, we used opacities from McKemmish et al. (2019), McKemmish et al. (2016), and Wende et al. (2010), respectively. For the remaining molecular species, the opacities were obtained from the DACE Opacity Database¹ using the Yadin line list (Yadin et al. 2012) for MgH, Rivlin line list (Rivlin et al. 2015) for CaH, and the MoLLIST line list (Burrows et al. 2002) for CrH.

4. RESULTS

4.1. The Dayside Spectra of TOI-1431 b and TOI-1518 b

We detect a significant Fe I signals in emission from both TOI-1431 b and TOI-1518 b. The fitting parameters (v_{sys} and K_P) that maximize the detection significance are consistent with those reported in previous literature (Addison et al. 2021; Cabot et al. 2021). The detected emission signals clearly indicate the presence of temperature inversions in the atmospheres of the two planets. We show the best-fit P-T profiles from the simple grid search, assuming a constant VMR of Fe I as a function of altitude, in Fig. 2. Both show a strong inversion as seen in other UHJs (e.g., Cont et al. 2021a; Johnson et al. 2023). We show the shifted and combined CCFs for TOI-1431 b in Fig. 3, and for TOI-1518 b in Figs. 4 and 5. The detected species, significance values, and best-fit VMRs for both planets are listed in Table 3, while the P-T profile parameters are listed in Tables 2. We again emphasize that these parameters have not been produced by a rigorous retrieval, and are likely subject to systematic effects due to simplifying assumptions.

In order to set limits upon the presence of TiO in both planets, we follow the same methodology as used by Johnson et al. (2023). Briefly, we injected a model spectrum using the TiO opacity tables produced by B. Plez and obtained from the petitRADTRANS opacity repository². We then attempted to retrieve the injected spectrum using a TiO model constructed from the line list of McKemmish et al. (2019), in order to attempt to mimic the effects of line list uncertainty. While such a procedure likely overestimates the detection significance (Johnson et al. 2023; Petz et al. 2024), this nonetheless

suggests that we should have been able to detect TiO if it was present in both planets with a VMR of $\gtrsim 10^{-9}$. This is well below the predicted equilibrium abundances from `FastChem`, and suggests that TiO is indeed depleted in both planets.

4.1.1. TOI-1431 b

For TOI-1431 b, Fe I and Cr I exceed the 4σ threshold. No other species among those searched rise above a threshold of 3σ . These are shown in Fig. 3. More data, ideally from the other side of secondary eclipse, will be necessary to search for other species.

4.1.2. TOI-1518 b

For TOI-1518 b, we make a firm detection ($> 4\sigma$) only of Fe I emission, with a significance of 7.92σ combining both of our nights. We show this detection in the upper left panel of Fig. 4.

We also make tentative detections of Fe II, Ni I, and Mg I, shown in Fig. 5. Ni I has a significance of $> 4\sigma$ when considering only the pre-eclipse observations, but this drops to 3.82σ when combining both nights of data. The significance of the Mg I signal also drops when the second night of data is added, but that of the Fe II signal remains approximately constant. We note that for Ni I and Mg I, we analyze only the PEPSI red-arm data; the Ni I lines are concentrated in the red arm, while the Mg I blue-arm data are dominated by the Mg I triplet and a strong alias with the Fe I signal, as previously seen for KELT-20 b by Petz et al. (2024). Any Mg I which might be seen in the blue arm is thus unreliable and we choose to exclude it from the analysis entirely.

There are several possibilities to explain the patterns shown by Fe II, Ni I, and Mg I. The SNR of the post-eclipse data is poorer than the pre-eclipse data (Fig. 1), and it is possible that the signals in this dataset are simply too weak to contribute to the combined signal; however, the Fe I detection significance increased modestly in the combined dataset. Alternately, it is possible that the true signal strength is changing as a function of time or phase. Borsa et al. (2022) argued for a similar phase-variable signal for Cr I and Fe II in KELT-20 b, but neither Kasper et al. (2023) nor Petz et al. (2024) could reproduce their detections. Petz et al. (2024) also found tentative evidence for a stronger pre-eclipse than post-eclipse Ni I signal in KELT-20 b, but the low signal significance prevented a firm conclusion.

We can explore the plausibility of such a phase variation with some simple models. In the pre-eclipse observations, we are viewing more of the afternoon hemisphere, which one might expect to be hotter than the morning hemisphere visible post-eclipse. All other things being equal, we might expect stronger pre-eclipse

¹ <https://dace.unige.ch/opacityDatabase/>

² <https://keeper.mpdl.mpg.de/d/e627411309ba4597a343/>

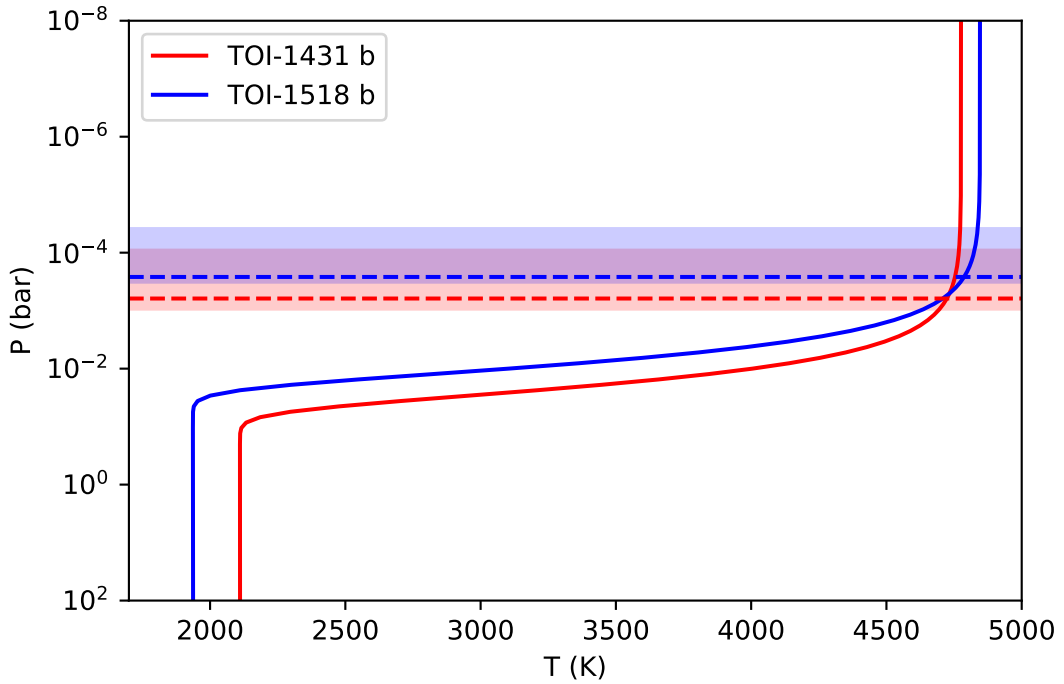


Figure 2. Pressure-temperature profiles for TOI-1431 b and TOI-1518 b adopted in this work, shown in red and blue, respectively. The horizontal dashed lines and bands show, in the same per-planet colors, the estimated pressure of peak of the contribution function and 68% contribution range for the Fe I emission spectrum, as calculated by `petitRADTRANS`.

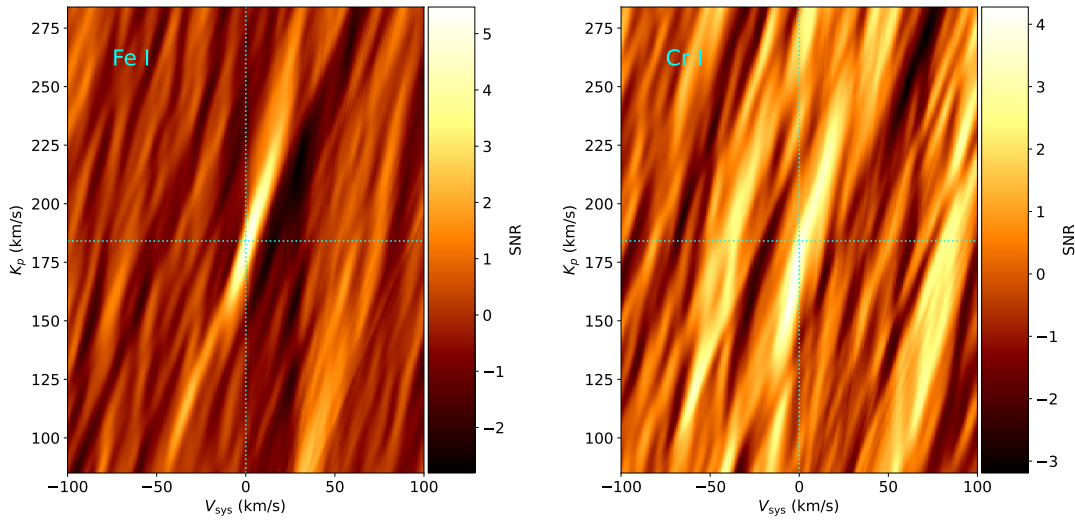


Figure 3. CCFs for TOI-1431 b, after being shifted into the planetary rest frame assuming a range of values of the planetary RV semi-amplitude K_p and combined. Fe I is shown on the left and Cr I on the right.

Table 2. System and Atmospheric Model Parameters

TOI-1431 b		TOI-1518 b		
	Value	Source	Value	Source
R_P (R_J)	1.49 ± 0.05	Addison et al. (2021)	1.875 ± 0.053	Cabot et al. (2021)
M_P (M_J)	3.12 ± 0.18	Addison et al. (2021)	< 2.3 (3σ limit)	Cabot et al. (2021)
T_{eq} (K)	2370 ± 70	Addison et al. (2021)	2492 ± 38	Cabot et al. (2021)
P (d)	$2.65023142 \pm 0.00000017$	Duck et al. (in prep)	1.9026055 ± 0.0000066	Duck et al. (in prep)
T_0 (BJD_TDB)	$22458712.674837 \pm 0.000072$	Duck et al. (in prep)	$2459854.41433 \pm 0.00012$	Duck et al. (in prep)
R_* (R_{\odot})	1.92 ± 0.07	Addison et al. (2021)	1.950 ± 0.048	Cabot et al. (2021)
M_* (M_{\odot})	$1.90^{+0.10}_{-0.08}$	Addison et al. (2021)	1.79 ± 0.26	Cabot et al. (2021)
T_{eff} (K)	7690^{+400}_{-250}	Addison et al. (2021)	7300 ± 100	Cabot et al. (2021)
K_P (km s^{-1}) [*]	187.4 ± 3.3	Addison et al. (2021)	203.7 ± 9.9	Cabot et al. (2021)
v_{sys} (km s^{-1}) [†]	-24.902 ± 0.011	This Work	-11.170 ± 0.035	This Work
$v \sin i_P$ (km s^{-1}) [*]	2.858 ± 0.096	Addison et al. (2021)	5.01 ± 0.14	Cabot et al. (2021)
κ_{IR}	0.005	This Work	0.04	This Work
γ	30	This Work	45	This Work
P_0 (bar)	1	...	1	...
X_{H_2}	0.7496	...	0.7496	...
X_{He}	0.2504	...	0.2504	...
VMR(H ⁻)	1×10^{-9}	...	1×10^{-9}	...
$N_{\text{SYSREM,Blue}}$	3	...	4	...
$N_{\text{SYSREM,Red}}$	1	...	3	...

NOTE—* The quoted value is derived from parameters given in the quoted work, but is not explicitly calculated in the reference.

[†] The quoted systemic velocity is measured in the PEPsi frame.

signals due to the larger flux from the hotter afternoon atmosphere. Cabot et al. (2021), however, found a day-side hot-spot offset consistent with zero from the *TESS* phase curve, questioning the viability of this interpretation. Changes in atmospheric abundances across the day-side due to thermal effects or photoionization could also affect the signal strength. In Fig. 6 we show the expected equilibrium abundances from `FastChem` at a pressure of 1 mbar. Ni should be primarily ionized above a temperature of ~ 3000 K, while Fe and Mg should be primarily ionized above ~ 3750 K. If we were indeed seeing varying signal strength due to thermal ionization in an afternoon hotspot, we would expect the signals of neutral species to be stronger post-eclipse and the ionized species stronger pre-eclipse. Instead, both the neutral species Mg I and Ni I and the ionized species Fe II appear to exhibit the same phase behavior, stronger in the pre-eclipse data, which is different from the behavior of the neutral species Fe I. `FastChem`, however, does not account for photoionization, which could be important for TOI-1518 b and its A-type host star. Confirming and interpreting a changing signal strength will require a fully Bayesian retrieval analysis and a more detailed model, both of which we will pursue in a future work.

Additionally, we see tentative detections of Cr I and CaH at a $3-4\sigma$ significance. There are, however, reasons for caution for both of these signals. For Cr I, the peak of the signal in the 2023 Nov. 6 data (lower left panel of Fig. 4) occurs at a K_P value approximately 50 km s $^{-1}$ lower than the expected value. While offsets in the peak K_P between different species have been seen in other planets and ascribed to atmospheric dynamics (Brogi et al. 2023; Cont et al. 2024, e.g.,[]), the discrepancy for Cr I is much larger than seen in other planets, raising the possibility that this is not a genuine planetary signal. CaH, meanwhile, has never before been observed in a hot Jupiter atmosphere. Its SNR is slightly lower in the combination of both datasets versus the 2023 Nov. 6 data. More data will be necessary to confirm or deny the presence of Cr I and CaH in the atmosphere of TOI-1518 b.

5. TEMPERATURE INVERSIONS IN THE POPULATION OF UHJs

Temperature inversions appear to be ubiquitous in the day-side atmospheres of UHJs; every UHJ that has been observed to date with high-resolution emission spectroscopy has shown Fe I and/or CO lines in emission (e.g., Pino et al. 2020; Yan et al. 2020, 2022, 2023; Nugroho et al. 2020; Borsa et al. 2022; Scandariato et al.

2023; Hoeijmakers et al. 2024; Cont et al. 2024). Cooler hot Jupiters, meanwhile, show absorption spectra indicating a monotonically decreasing temperature profile (e.g., Brogi et al. 2014; Birkby et al. 2017; Rasmussen et al. 2022; Smith et al. 2023). With the increasing population of planets observed in emission spectroscopy, we can start to consider population-level questions, including: above which temperature do planets have inverted atmospheres? Is there also a dependence on other parameters, such as surface gravity? What does this tell us about what absorbers are responsible for the presence of inversions?

To begin to answer these questions, we perform a literature search of HJs and investigate their physical properties. In Table 4 we list properties from the literature of the sample of HJs with emission spectroscopy indicating the presence or absence of a temperature inversion. This sample of planets consists not only of those observed with high-resolution spectroscopy, but also planets where low-resolution space-based emission spectroscopy with *Hubble* or *JWST* has allowed retrieval of the temperature-pressure profile (e.g., Mikal-Evans et al. 2019; Wong et al. 2016).

We note that high and low resolution spectroscopy probe different pressure levels in the atmosphere, with higher-resolution spectra probing higher in the atmosphere. In principle, it might be possible for one to reach different conclusions about the P-T profile from high versus low-resolution data if e.g. there is an inversion high in the atmosphere but a decreasing profile deeper in the atmosphere. For the six planets with both and high resolution spectra, however: WASP-33 b (Haynes et al. 2015; Yan et al. 2022), WASP-121 b (Mikal-Evans et al. 2019; Hoeijmakers et al. 2024), WASP-18 b (Yan et al. 2023; Brogi et al. 2023), KELT-20 b (Cont et al. 2021a; Fu et al. 2022a), WASP-76 b (West et al. 2016; Yan et al. 2023), and WASP-77 Ab (Smith et al. 2023; August et al. 2023), the two methods agree that the five hotter planets possess temperature inversions, while the cooler WASP-77 Ab does not. One other caveat is that, at high T_{eq} , a planet with an inverted P-T profile might show a featureless *Hubble* spectrum because this covers the $1.4\mu\text{m}$ water feature, which might vanish due to dissociation of H₂O and/or continuum opacity due to H⁺ (e.g., Parmentier et al. 2018).

Additionally, in order to fill out the low T_{eq} end of our sample, we included four non-transiting HJs for which high-resolution infrared spectroscopy has revealed molecular absorption lines and therefore the lack of a temperature inversion: τ Boo b (Pelletier et al. 2021), HD 179949 b (Brogi et al. 2014), 51 Peg b (Birkby et al. 2017), and HD 102915 b (Guilluy et al. 2019). As these

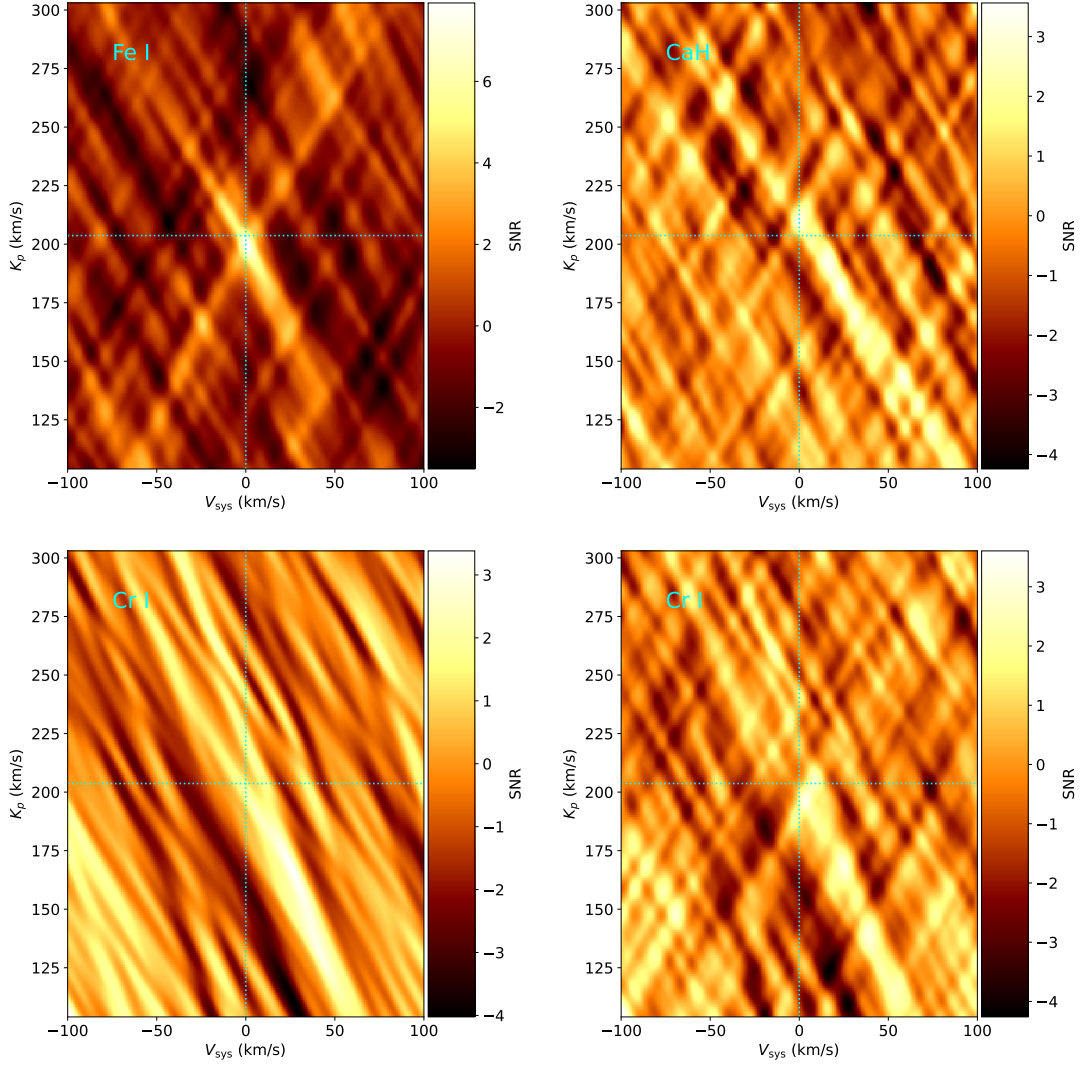


Figure 4. Shifted and combined CCFs for TOI-1518 b for Fe I (top left), CaH (top right), and Cr I (bottom row). For the bottom row, the left plot shows only the data from 2023 Nov. 6, while the right plot shows both nights. These plots combine the PEPSI red and blue arms, except for CaH, which shows the blue arm only.

planets are non-transiting, however, we do not know the radius and therefore the surface gravity. Instead, we make use of the relation between irradiation, mass, and radius for HJs to estimate plausible values for their radii. Using the NASA Exoplanet Archive³, we identify the ten closest transiting planets to each of the aforementioned planets in $T_{\text{eq}}-M_P$ space. Then, we use the mean and standard deviation of the radii of these ten planets as the estimated radius and uncertainty of the planet in question. We list these values in Table 4.

Following Beatty et al. (2017b) and Parmentier et al. (2018), we investigate the relationship between equilibrium temperature (T_{eq}) and surface gravity (g_P) with

these planets using our sample with a broader parameter space (Figure 7). Surface gravity may be important to the presence of inversions because the chemical agent responsible for the inversions may condense and rain out on the cool night side of the planet, a process which is expected to be more efficient at higher surface gravity (Beatty et al. 2017a,b). Beatty et al. (2017b) proposed a model where the presence or absence of an inversion is dependent primarily on the surface gravity, with only a small dependence upon temperature, at least over the range between 1700 and 3500 K that they considered. Parmentier et al. (2018), meanwhile, considered the parts of parameter space where gaseous TiO should occur, and where there should be H⁻ continuum absorption, which has also been suggested to be responsible for

³ <https://exoplanetarchive.ipac.caltech.edu/>

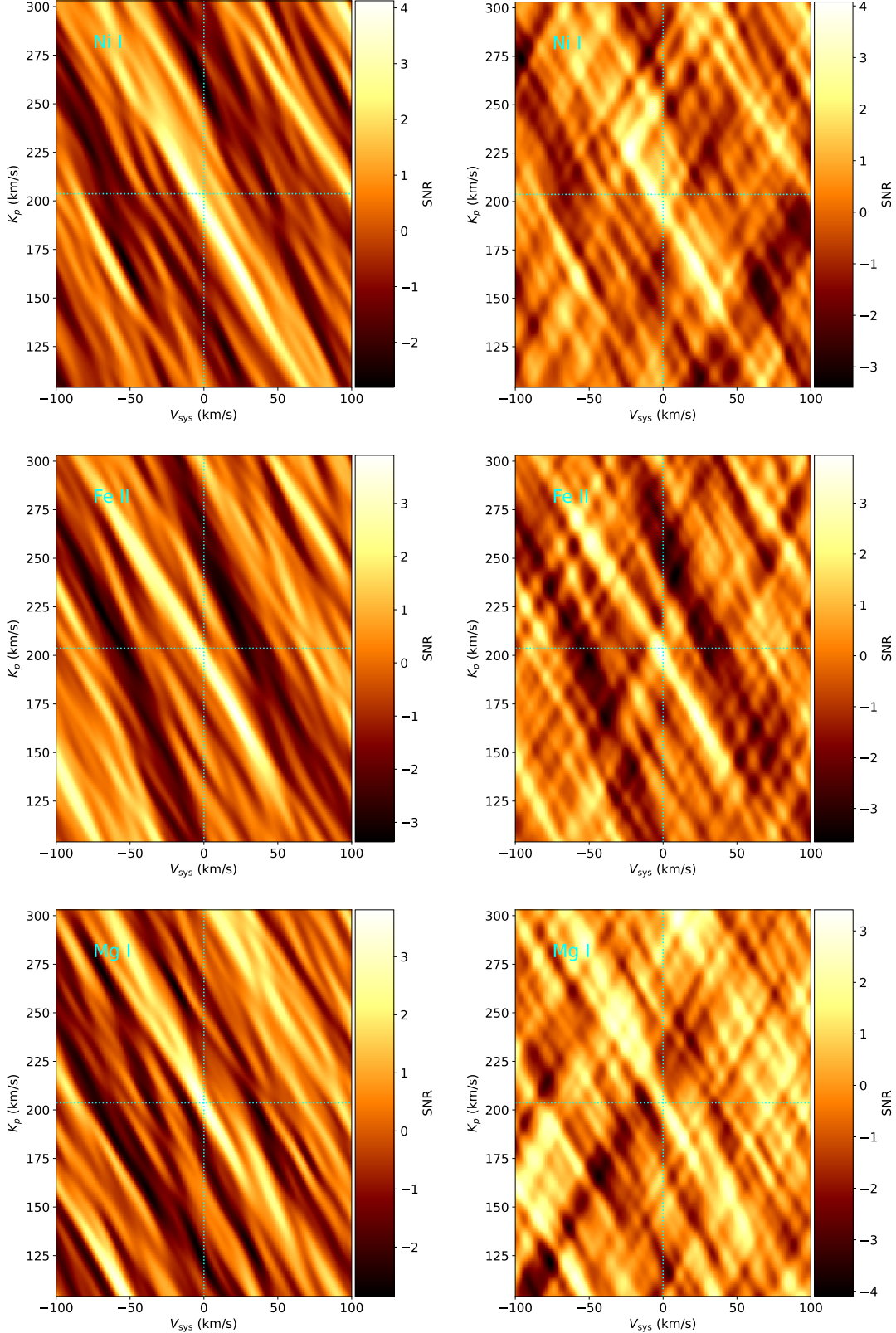


Figure 5. Shifted and combined CCFs for TOI-1518 b for Ni I (top row), Fe II (middle row), and Mg I (bottom row) for only the 2023 Nov. 6 observations (left column) and for the combined datasets (right column). The data for Fe II use both PEPSI arms, while those for Ni I and Mg I use only the red arm. The detection strengths *decrease* in the combined data, perhaps indicating a changing signal strength between the two datasets. See the main text for further discussion.

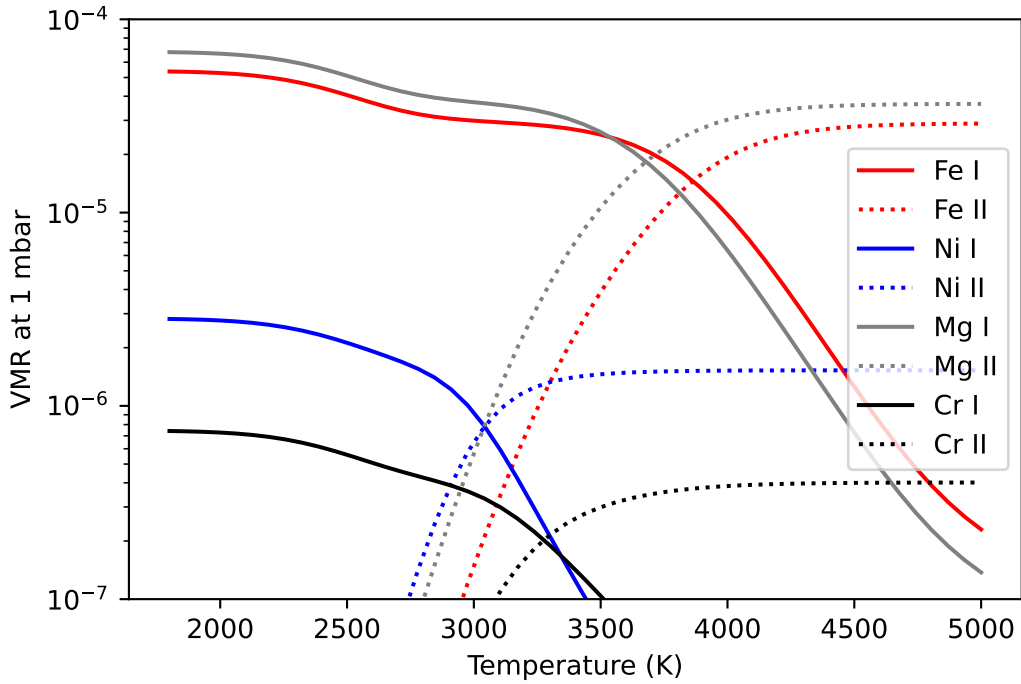


Figure 6. Expected VMR at a pressure of 1 mbar across a range of temperatures possible for the upper atmosphere of TOI-1518 b, as calculated by `FastChem`. Neutral species are shown as solid lines, and the corresponding singly ionized species as dotted lines.

Table 3. Summary of Results

Species	TOI-1431 b		TOI-1518 b		VMR
	SNR (σ)	VMR	SNR (σ)	SNR (σ)	
	both dates		2023-11-06 UT		
Fe I	5.40	5.47×10^{-5}	7.92	6.69	3.2×10^{-4}
Fe II	2.45	2.90×10^{-5}	3.94	3.91	3.2×10^{-4}
Ni I	2.00	2.77×10^{-6}	3.82	4.13	3.2×10^{-5}
Mg I	1.41	6.76×10^{-5}	3.11	3.81	6.8×10^{-4}
Cr I	4.23	7.35×10^{-7}	3.52	2.54	3.2×10^{-6}
CaH	1.78	1.81×10^{-6}	3.26	3.51	5.6×10^{-6}

NOTE—For TOI-1518 b, the “both dates” column lists the peak SNR for the species combining the data from both datasets, while the “2023 Nov. 6 UT” columns lists the SNR only considering data from that date. The quoted VMR is that which maximizes the detection significance and should not be taken as a robust measurement. See the main text for more discussion.

inversions (Lothringer et al. 2018). These domains are also shown in Fig. 7.

As can be seen in Fig. 7, planets with and without inversion separate into distinct parts of the $T_{\text{eq}} - g_P$ space. For planets with moderate to low surface gravity $g_P < 2g_J$ ($\log g = 3.695$), every planet with $T_{\text{eq}} > 2050$ K has an inverted atmosphere, while no planet with $T_{\text{eq}} < 1950$ K does. Two planets with isothermal upper atmospheres observed by *Hubble* (HAT-P-31 Ab and HAT-P-41 b; Nikolov et al. 2018; Fu et al. 2022b) appear at temperatures near 1950 K and low surface gravity. At high surface gravity, the pattern is less clear, and only three objects fill out this space. Kepler-13 Ab and KELT-1 b both have non-inverted atmospheres despite having T_{eq} values above 2050 K, while WASP-18 b *does* have an inversion despite having T_{eq} and g_P values intermediate between the other two objects.

Comparing our sample to the predictions made by previous literature (Fig. 7), it is clear that with the addition of more recently observed HJs, these predictions do not match the current population. A significant number of planets with inverted spectra now occupy the regions predicted by Beatty et al. (2017b) to have ambiguous or absorption spectra, and WASP-18 b shows that the relationship between surface gravity and presence of an inversion is non-monotonic. Meanwhile, three planets with inversions are now known that are cooler than the point at which Parmentier et al. (2018) expected TiO to be effective: KELT-20 b, WASP-76 b, and KELT-7 b, while WASP-18 b is too high surface gravity to be expected to have TiO.

We also compare to more recent models that use the three-dimensional non-grey global circulation model (GCM) grid presented by Roth et al. (2024). They simulated 345 planets spanning a wide range of parameters that are typical for HJs including temperature and surface gravity, but also including stellar mass, planetary metallicity, magnetic drag strength, and presence or absence of TiO. They provided global P-T profiles, spanning 64 longitudinal points, 32 latitudinal points and 53 pressure levels. For simplicity, we select the P-T profile of the substellar point for each simulated planet, as this region should dominate the emission spectrum. In order to marginalize over the other parameters, not all of which are known for the planets in our observational sample, we simply collapse the grid into $T_{\text{eq}} - g_P$ space by evaluating the average slope of all the simulated P-T profiles between 0.1 and 10 mbar at each $T_{\text{eq}} - g_P$ grid point. The models including TiO predict the presence of inversions at low T_{eq} and diminishing towards higher T_{eq} , the opposite of the observed distribution, and so we exclude these models from further analysis. In Fig. 8

we show contours of this average slope, where negative slopes imply a temperature inversion and positive slopes imply a decreasing P-T profile. These contours appear to match reasonably well with the observed population with moderate to low surface gravity, although it predicts the transition from non-inverted to inverted profiles at a temperature ~ 200 K higher than observed. Additionally, the surface gravity range covered by the model grid ($\log g = 0.8 - 1.8$) does not include our high gravity objects like Kepler-13 Ab and WASP-18 b.

As an additional test of potential inversion agents, we compute chemical models using the *FastChemCond* code (Stock et al. 2018, 2022; Kitzmann et al. 2024) in order to compute equilibrium chemical abundances in these atmospheres, accounting for condensation of condensable species. We concentrate on a pressure level of 10^{-2} bar, similar to the location where our data suggests the inversions in TOI-1431 b and TOI-1518 b may occur (Fig. 2). We compute the expected VMRs of Fe I, Ni I, TiO, VO, and H⁻ between temperatures of 500 and 4000 K.

We show the expected VMRs of these species in the bottom panel of Fig. 8. In order for a single species to be responsible for the inversions, we would expect it to have a significant VMR starting between 1950 and 2050 K, and remaining in gaseous form at higher temperatures. As is apparent from Fig. 8, the best match appears to be TiO; Fe I, Ni I, and VO would all be expected to be gaseous at the temperatures of known non-inverted planets like WASP-77 Ab and τ Boo b, while H⁻ does not reach significant VMRs until temperatures in excess of 2500 K. From this perspective, it seems that TiO may be the most likely cause of the temperature inversions in UHJs. Nonetheless, despite extensive searches over the past decade, observational evidence for the presence of TiO in HJ atmospheres is lacking. Prineth et al. (2022) detected TiO in transmission in WASP-189 b, while potential detections in WASP-33 b have been controversial (Nugroho et al. 2017; Cont et al. 2021b; Herman et al. 2020; Serindag et al. 2021). On the other side, we did not detect TiO in either TOI-1431 b nor TOI-1518 b and set stringent limits on the VMR of $\sim 10^{-9}$, two order of magnitude below the expected equilibrium concentration; there are also tight limits for other UHJs (e.g., Johnson et al. 2023). Finally, the GCM suite including TiO absorption produced by Roth et al. (2024) provides a poor match to the population of HJ inversions, while their TiO-free models provides a reasonable match.

Empirically, every UHJ with a temperature inversion observed in the optical shows strong Fe I emission lines (e.g., Pino et al. 2020; Yan et al. 2020; Nugroho et al. 2020; Borsa et al. 2022; Scandariato et al. 2023; Hoei-

jmakers et al. 2024). Atomic opacity, including Fe I, has been proposed as a possible source of inversions (Lothringer et al. 2018). While the `FastChemCond` chemical model for the presence of Fe I vapor does not match the observed population, we caution that this is a relatively simple, equilibrium chemistry model, and does not account for processes such as atmospheric mixing, photoionization, or the inherently three-dimensional nature of planets.

While Fe I appears to be the main species responsible for temperature inversions rather than TiO, more observations of planets across the parameter space and more detailed atmospheric models are necessary to test the boundaries of the inverted versus non-inverted regimes and to further determine which species are responsible for temperature inversions in UHJs.

6. CONCLUSIONS

We have presented high-resolution optical emission spectra of the ultra hot Jupiters TOI-1431 b and TOI-1518 b with LBT/PEPSI (§2). Using a cross-correlation analysis (§3), we detect strong signals of Fe I emission lines for both planets (5.40σ and 7.92σ ; §4.1), as well as Cr I for TOI-1431 b (4.23σ ; §4.1.1). We also find tentative detections of $3 - 4\sigma$ for several other species in TOI-1518 b (§4.1.2). In the latter planet, there is possible evidence of a change in the strength of the tentative Fe II, Ni I, and Mg I signals between our pre- and post-eclipse datasets, but a more careful Bayesian analysis and/or more data will be necessary to confirm or refute this possibility.

The Fe I emission lines from TOI-1431 b and TOI-1518 b show that these planets both have temperature inversions in their dayside atmospheres. These add to the ubiquity of both temperature inversions and of optical spectra dominated by Fe I emission among UHJs at low to moderate surface gravity. We have conducted an analysis of the population of HJs (§5) by collecting literature values. We display the population as a function of planetary equilibrium temperature T_{eq} and surface gravity g_P . Previous models proposed by Beatty et al. (2017b) and Parmentier et al. (2018) for the distribution of inversions in this space do not match the current population (Fig. 7), but a recent GCM suite from Roth et al. (2024) provides a better match (Fig. 8). While simple equilibrium chemical models from `FastChemCond` suggest that the distribution of TiO as a function of T_{eq}

best matches the pattern seen in the population, but this is challenged by the small number of detections of TiO in these planets (e.g., Johnson et al. 2023). Alternately, given that Fe I emission seems to be ubiquitous in the optical spectra of UHJs observed to date, Fe I may in fact be responsible for the presence of the inversions, as proposed by Lothringer et al. (2018). Future emission observations of more HJs in order to probe the presence of inverted atmospheres, or lack thereof, will help to define the limits of the parameter space where inversions occur, as well as further constrain which chemical species may cause the inversions. Particularly needed are planets with intermediate equilibrium temperatures ($1750 \text{ K} < T_{\text{eq}} < 2200 \text{ K}$) and high surface gravity ($g_P > 2g_J$). Even bright non-transiting HJs could be appropriate targets for such observations, particularly with the advent of recent infrared spectra like CRIRES+ and KPIC which are capable of detecting molecules like H₂O and CO found across the T_{eq} range (e.g., Cont et al. 2024; Finnerty et al. 2024).

The PEPSI spectra used in this paper will be made publicly available through the NASA Exoplanet Archive⁴.

We thank the LBT support astronomers, telescope operators, and observers who helped to gather our data: Alex Becker, Andrew Cardwell, Steve Allanson, Josh Williams, Mark Whittle, Peter Garnavich, Don Terndrup, and Michael Tucker. Thanks to Scott Gaudi and Thomas Beatty for useful discussions.

MCJ is supported by NASA Grant 80NSSC23K0692.

The LBT is an international collaboration among institutions in the United States, Italy and Germany. LBT Corporation Members are: The Ohio State University, representing OSU, University of Notre Dame, University of Minnesota and University of Virginia; LBT Beteiligungsgesellschaft, Germany, representing the Max-Planck Society, The Leibniz Institute for Astrophysics Potsdam, and Heidelberg University; The University of Arizona on behalf of the Arizona Board of Regents; and the Istituto Nazionale di Astrofisica, Italy.

Facilities: LBT(PEPSI)

Software: astropy (Astropy Collaboration et al. 2013, 2018), `petitRADTRANS` (Mollière et al. 2019), `FastChemCond` (Stock et al. 2018, 2022; Kitzmann et al. 2024), `SpectroscopyMadeEasy` (Valenti & Piskunov 1996, 2012), SDS4PEPSI (Ilyin 2000; Strassmeier et al. 2018)

Table 4. Temperature Inversions in Hot Jupiters

Planet	HRS	LRS	References	T_{eq} (K)	M_P (M_J)	R_P (R_J)	Surface Gravity (log g)
KELT-9 b	Inv	...	1; 2	4050 ± 180	2.88 ± 0.84	$1.891^{+0.061}_{-0.053}$	3.297 ± 0.130
WASP-189 b	Inv	...	3; 4	3353^{+27}_{-34}	$1.99^{+0.16}_{-0.14}$	1.619 ± 0.021	3.275 ± 0.034
WASP-33 b	Inv	Inv	4; 5; 57	2782 ± 41	2.093 ± 0.139	1.593 ± 0.074	3.308 ± 0.048
WASP-121 b	Inv	Inv	6; 7; 60	2720 ± 8	1.157 ± 0.070	1.753 ± 0.036	2.969 ± 0.032
HAT-P-7 b	...	Inv	8; 9; 10	2700	1.84 ± 0.53	1.51 ± 0.21	3.303 ± 0.172
MASCARA-1 b	Inv	...	11; 12	$2594.3^{+1.6}_{-1.5}$	3.7 ± 0.9	$1.597^{+0.018}_{-0.019}$	3.556 ± 0.105
WASP-12 b	...	Inv	5; 13	2592.6 ± 57.2	1.465 ± 0.079	1.937 ± 0.056	2.985 ± 0.035
Kepler-13 Ab	...	Dec	14; 15	2550 ± 80	9.28 ± 0.16	1.512 ± 0.035	4.003 ± 0.021
WASP-103 b	...	Inv	16; 17	2508^{+75}_{-70}	1.490 ± 0.088	$1.528^{+0.073}_{-0.047}$	3.200 ± 0.034
TOI-1518 b	Inv	...	18; This Work	2492 ± 38	<2.3	1.875 ± 0.053	$3.207^{+0.027}_{-0.434}$
WASP-178 b	Inv	...	55; 56	2470 ± 60	1.66 ± 0.12	1.81 ± 0.09	3.102 ± 0.051
WASP-18 b	Inv	Inv	19; 20; 21; 22; 41	2429^{+77}_{-70}	10.20 ± 0.35	1.240 ± 0.079	4.214 ± 0.059
TOI-1431 b	Inv	...	23; This Work	2370 ± 70	3.12 ± 0.18	1.49 ± 0.05	3.540 ± 0.037
KELT-20 b	Inv	Inv	24; 25; 42; 43	2262 ± 73	<3.382	$1.741^{+0.069}_{-0.074}$	$3.440^{+0.035}_{-0.430}$
KELT-1 b	...	Dec	26; 27	2233.35	$27.23^{+0.50}_{-0.48}$	$1.110^{+0.032}_{-0.022}$	$4.739^{+0.026}_{-0.020}$
WASP-76 b	Inv	Inv	28; 29; 21	2160 ± 40	0.92 ± 0.03	$1.83^{+0.06}_{-0.04}$	$2.826^{+0.032}_{-0.024}$
KELT-7 b	...	Inv	30; 9; 31	2048 ± 27	1.39 ± 0.22	1.60 ± 0.06	3.127 ± 0.080
HAT-P-41 b	...	Iso	9; 46; 47	1941 ± 38	1.19 ± 0.60	2.05 ± 0.50	2.841 ± 0.310
WASP-74 b	...	Dec	9; 53; 54	1926 ± 21	0.72 ± 0.12	1.26 ± 0.10	2.985 ± 0.100
HAT-P-32 Ab	...	Iso	48; 49	$1835.7^{+0.110}_{-0.062}$	$0.68^{+0.11}_{-0.10}$	1.98 ± 0.045	$2.632^{+0.073}_{-0.068}$
WASP-79 b	...	Dec	52	$1716^{+25.8}_{-24.4}$	0.85 ± 0.08	1.53 ± 0.04	2.857 ± 0.075
WASP-77 Ab	Dec	Dec	20; 32; 44	1715^{+26}_{-25}	$1.667^{+0.068}_{-0.064}$	$1.230^{+0.031}_{-0.029}$	3.436 ± 0.028
WASP-101 b	...	Dec	9; 50; 51	1560 ± 35	0.51 ± 0.08	1.43 ± 0.09	2.913 ± 0.079
HD 209458 b	Dec	...	9; 33	1484 ± 18	0.73 ± 0.04	1.39 ± 0.02	2.972 ± 0.264
HIP 65 Ab	Dec	...	45	1411 ± 15	3.213 ± 0.078	$2.03^{+0.61}_{-0.49}$	$3.297^{+0.271}_{-0.217}$
HD 189733 b	Dec	...	34; 35	1209 ± 11	$1.166^{+0.052}_{-0.049}$	1.119 ± 0.038	$3.363^{+0.374}_{-0.327}$
WASP-69 b	...	Dec	9; 58; 59	963 ± 18	0.29 ± 0.03	1.11 ± 0.04	2.765 ± 0.055
τ Boo b	Dec	...	36	1661 ± 70	6.24 ± 0.23	1.115 ± 0.092	3.292 ± 0.071
HD 179949 b	Dec	...	37; 38	1591 ± 30	0.98 ± 0.04	1.28 ± 0.15	3.172 ± 0.101
51 Peg b	Dec	...	39; 38	1318 ± 46	$0.476^{+0.032}_{-0.031}$	1.15 ± 0.22	2.951 ± 0.169
HD 102195 b	Dec	...	40	1054 ± 13	0.46 ± 0.03	1.11 ± 0.20	2.985 ± 0.156

NOTE—Sample of hot Jupiters from the literature used in the analysis described in §5 and shown in Fig. 7 and Fig. 8. The sample is listed in descending order of equilibrium temperature. Planets above the line are transiting planets, while those below the line are non-transiting and we have estimated the planetary radius and surface gravity as described in the main text. The columns “HRS” and “LRS” denote whether the planet has been observed with high or low resolution, respectively. These observations have resulted in the detection of an inversion (Inv), a decreasing temperature profile (Dec), or an isothermal profile (Iso); an ellipsis denotes no data. References: 1: Gaudi et al. (2017); 2: Pino et al. (2020); 3: Lendl et al. (2020); 4: Yan et al. (2022); 5: Chakrabarty & Sengupta (2019); 6: Bourrier et al. (2020); 7: Mikal-Evans et al. (2019); 8: Wong et al. (2016); 9: Stassun et al. (2017); 10: Mansfield et al. (2018); 11: Hooton et al. (2022); 12: Ramkumar et al. (2023); 13: Arcangeli et al. (2021); 14: Esteves et al. (2015); 15: Beatty et al. (2017b); 16: Gillon et al. (2014); 17: Cartier et al. (2017); 18: Cabot et al. (2021); 19: Arcangeli et al. (2018); 20: Cortés-Zuleta et al. (2020); 21: Yan et al. (2023); 22: Coulombe et al. (2023); 23: Addison et al. (2021); 24: Lund et al. (2017); 25: Johnson et al. (2023); 26: Siverd et al. (2012); 27: Beatty et al. (2017a); 28: West et al. (2016); 29: Edwards et al. (2020); 30: Bieryla et al. (2015); 31: Pluriel et al. (2020); 32: Smith et al. (2023); 33: Rasmussen et al. (2022); 34: Birkby et al. (2013); 35: Addison et al. (2019); 36: Pelletier et al. (2021); 37: Brogi et al. (2014); 38: Rosenthal et al. (2021); 39: Birkby et al. (2017); 40: Guilluy et al. (2019); 41: Brogi et al. (2023); 42: Cont et al. (2021a); 43: Fu et al. (2022a); 44: August et al. (2023); 45: Bazinet et al. (2024), 46: Hartman et al. (2012); 47: Fu et al. (2022b); 48: Nikolov et al. (2018); 49: Wang et al. (2019); 50: Hellier et al. (2014); 51: Rathcke et al. (2023); 52: Gressier et al. (2023); 53: Mancini et al. (2019); 54: Fu et al. (2021); 55: Hellier et al. (2019); 56: Cont et al. (2024); 57: Haynes et al. (2015); 58: Casasayas-Barris et al. (2017); 59: Schlawin et al. (2024); 60: Hoeijmakers et al. (2024).

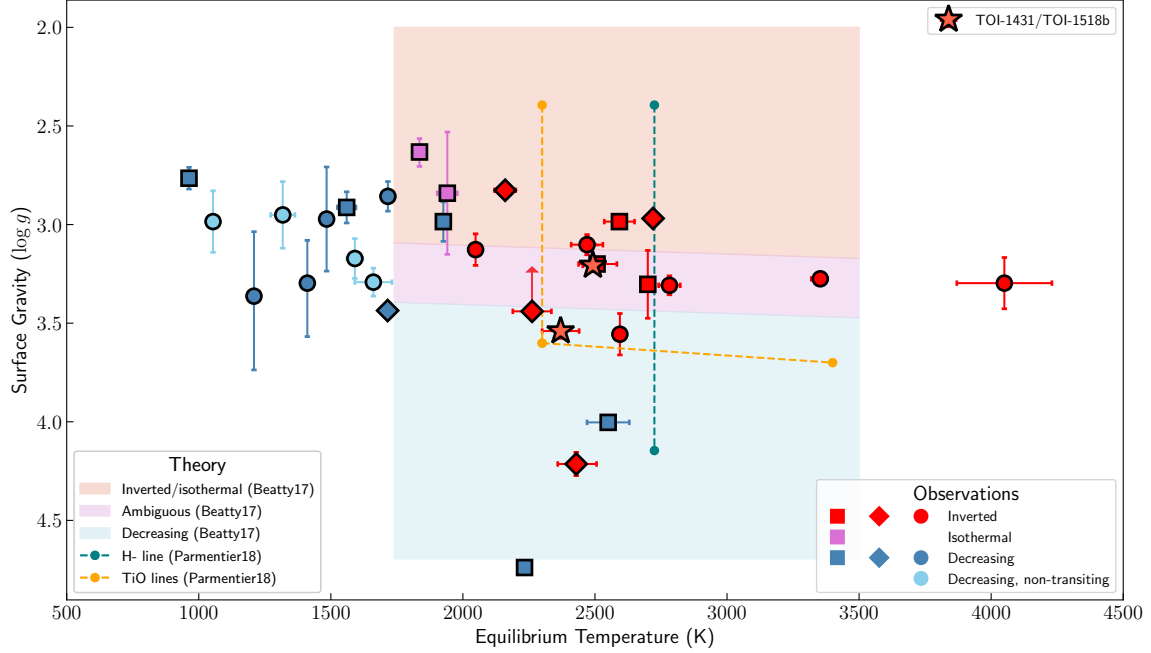


Figure 7. Surface gravity as a function of equilibrium temperature of HJs listed in Table 4. Circle, square, and diamond symbols represent planets observed in high resolution, low resolution, and both, respectively. The orange, purple, and blue shaded regions indicate regions of parameter space proposed by Beatty et al. (2017b) to host planets with inverted or isothermal, ambiguous, and monotonically decreasing P-T profiles, respectively. Note that Beatty et al. (2017b) cast these in terms of the dayside brightness temperature T_B which is a measured quantity not equal to the theoretical quantity T_{eq} which we use; however, their relation has only a weak dependence on temperature so the difference should be small. The yellow and teal dashed lines show the boundary found by Parmentier et al. (2018) for the presence of TiO and H^- , respectively; these species should be present above and to the right of these lines.

REFERENCES

Addison, B., Wright, D. J., Wittenmyer, R. A., et al. 2019, PASP, 131, 115003, doi: [10.1088/1538-3873/ab03aa](https://doi.org/10.1088/1538-3873/ab03aa)

Addison, B. C., Knudstrup, E., Wong, I., et al. 2021, AJ, 162, 292, doi: [10.3847/1538-3881/ac224e](https://doi.org/10.3847/1538-3881/ac224e)

Arcangeli, J., Désert, J. M., Parmentier, V., Tsai, S. M., & Stevenson, K. B. 2021, A&A, 646, A94, doi: [10.1051/0004-6361/202038865](https://doi.org/10.1051/0004-6361/202038865)

Arcangeli, J., Désert, J.-M., Line, M. R., et al. 2018, ApJL, 855, L30, doi: [10.3847/2041-8213/aab272](https://doi.org/10.3847/2041-8213/aab272)

Astropy Collaboration, Robitaille, T. P., Tollerud, E. J., et al. 2013, A&A, 558, A33, doi: [10.1051/0004-6361/201322068](https://doi.org/10.1051/0004-6361/201322068)

Astropy Collaboration, Price-Whelan, A. M., Sipőcz, B. M., et al. 2018, AJ, 156, 123, doi: [10.3847/1538-3881/aabc4f](https://doi.org/10.3847/1538-3881/aabc4f)

August, P. C., Bean, J. L., Zhang, M., et al. 2023, ApJL, 953, L24, doi: [10.3847/2041-8213/ace828](https://doi.org/10.3847/2041-8213/ace828)

Bazinet, L., Pelletier, S., Benneke, B., Salinas, R., & Mace, G. N. 2024, arXiv e-prints, arXiv:2403.07983, doi: [10.48550/arXiv.2403.07983](https://doi.org/10.48550/arXiv.2403.07983)

Beatty, T. G., Madhusudhan, N., Pogge, R., et al. 2017a, AJ, 154, 242, doi: [10.3847/1538-3881/aa94cf](https://doi.org/10.3847/1538-3881/aa94cf)

Beatty, T. G., Madhusudhan, N., Tsiaras, A., et al. 2017b, AJ, 154, 158, doi: [10.3847/1538-3881/aa899b](https://doi.org/10.3847/1538-3881/aa899b)

Bieryla, A., Collins, K., Beatty, T. G., et al. 2015, AJ, 150, 12, doi: [10.1088/0004-6256/150/1/12](https://doi.org/10.1088/0004-6256/150/1/12)

Birkby, J. L., de Kok, R. J., Brogi, M., et al. 2013, MNRAS, 436, L35, doi: [10.1093/mnrasl/slt107](https://doi.org/10.1093/mnrasl/slt107)

Birkby, J. L., de Kok, R. J., Brogi, M., Schwarz, H., & Snellen, I. A. G. 2017, AJ, 153, 138, doi: [10.3847/1538-3881/aa5c87](https://doi.org/10.3847/1538-3881/aa5c87)

⁴ <https://exoplanetarchive.ipac.caltech.edu/docs/PEPSIMission.html>

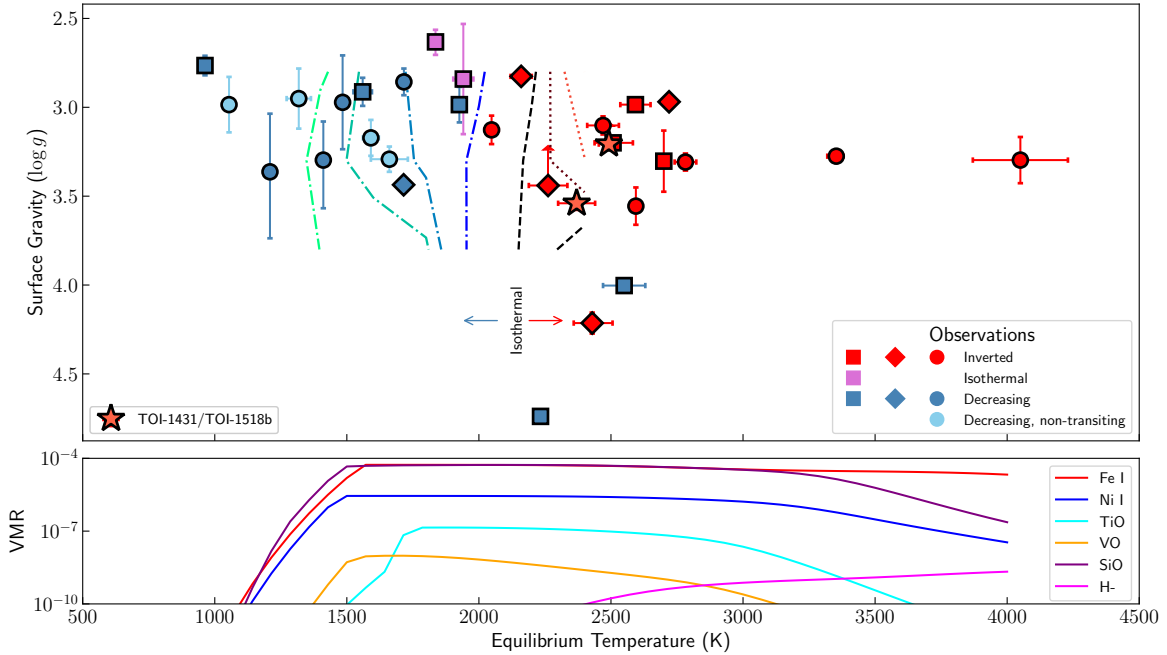


Figure 8. Top: same as Fig. 7, except showing contours of P-T profile slope derived from the GCM suite of Roth et al. (2024). The black dashed line shows the point at which an isothermal P-T profile is expected, while successively more blue-green (red) colors show successively more strongly decreasing (inverted) P-T profiles. The Roth et al. (2024) GCM grid only covers a limited range of $T_{\text{eq}} - g_P$ space as compared to the observed planets. We choose to use the grids excluding TiO as these grids predict non-inverted atmospheres towards higher T_{eq} . Bottom: expected volume mixing ratios at a pressure level of 10^{-2} bar of several proposed inversion agents as a function of planetary equilibrium temperature, as calculated with `FastChemCond`.

Borsa, F., Giacobbe, P., Bonomo, A. S., et al. 2022, *A&A*, 663, A141, doi: [10.1051/0004-6361/202142768](https://doi.org/10.1051/0004-6361/202142768)

Bourrier, V., Ehrenreich, D., Lendl, M., et al. 2020, *A&A*, 635, A205, doi: [10.1051/0004-6361/201936640](https://doi.org/10.1051/0004-6361/201936640)

Brogi, M., de Kok, R. J., Birkby, J. L., Schwarz, H., & Snellen, I. A. G. 2014, *A&A*, 565, A124, doi: [10.1051/0004-6361/201423537](https://doi.org/10.1051/0004-6361/201423537)

Brogi, M., Emeka-Okafor, V., Line, M. R., et al. 2023, *AJ*, 165, 91, doi: [10.3847/1538-3881/acaf5c](https://doi.org/10.3847/1538-3881/acaf5c)

Burrows, A., Ram, R. S., Bernath, P., Sharp, C. M., & Milsom, J. A. 2002, *ApJ*, 577, 986, doi: [10.1086/342242](https://doi.org/10.1086/342242)

Cabot, S. H. C., Bello-Arufe, A., Mendonça, J. M., et al. 2021, *AJ*, 162, 218, doi: [10.3847/1538-3881/ac1ba3](https://doi.org/10.3847/1538-3881/ac1ba3)

Cartier, K. M. S., Beatty, T. G., Zhao, M., et al. 2017, *AJ*, 153, 34, doi: [10.3847/1538-3881/153/1/34](https://doi.org/10.3847/1538-3881/153/1/34)

Casasayas-Barris, N., Palle, E., Nowak, G., et al. 2017, *A&A*, 608, A135, doi: [10.1051/0004-6361/201731956](https://doi.org/10.1051/0004-6361/201731956)

Chakrabarty, A., & Sengupta, S. 2019, *AJ*, 158, 39, doi: [10.3847/1538-3881/ab24dd](https://doi.org/10.3847/1538-3881/ab24dd)

Cont, D., Yan, F., Reiners, A., et al. 2021a, arXiv e-prints, arXiv:2112.10461. <https://arxiv.org/abs/2112.10461>

—. 2021b, *A&A*, 651, A33,

doi: [10.1051/0004-6361/202140732](https://doi.org/10.1051/0004-6361/202140732)

Cont, D., Nortmann, L., Yan, F., et al. 2024, arXiv e-prints, arXiv:2406.08166, doi: [10.48550/arXiv.2406.08166](https://doi.org/10.48550/arXiv.2406.08166)

Cortés-Zuleta, P., Rojo, P., Wang, S., et al. 2020, *A&A*, 636, A98, doi: [10.1051/0004-6361/201936279](https://doi.org/10.1051/0004-6361/201936279)

Coulombe, L.-P., Benneke, B., Challener, R., et al. 2023, *Nature*, 620, 292, doi: [10.1038/s41586-023-06230-1](https://doi.org/10.1038/s41586-023-06230-1)

Eastman, J. D., Rodriguez, J. E., Agol, E., et al. 2019, arXiv e-prints, arXiv:1907.09480, doi: [10.48550/arXiv.1907.09480](https://doi.org/10.48550/arXiv.1907.09480)

Edwards, B., Changeat, Q., Baeyens, R., et al. 2020, *AJ*, 160, 8, doi: [10.3847/1538-3881/ab9225](https://doi.org/10.3847/1538-3881/ab9225)

Esteves, L. J., De Mooij, E. J. W., & Jayawardhana, R. 2015, *ApJ*, 804, 150, doi: [10.1088/0004-637X/804/2/150](https://doi.org/10.1088/0004-637X/804/2/150)

Finnerty, L., Xuan, J. W., Xin, Y., et al. 2024, *AJ*, 167, 43, doi: [10.3847/1538-3881/ad1180](https://doi.org/10.3847/1538-3881/ad1180)

Flagg, L., Turner, J. D., Deibert, E., et al. 2023, *ApJL*, 953, L19, doi: [10.3847/2041-8213/ace529](https://doi.org/10.3847/2041-8213/ace529)

Fortney, J. J., Lodders, K., Marley, M. S., & Freedman, R. S. 2008, *ApJ*, 678, 1419, doi: [10.1086/528370](https://doi.org/10.1086/528370)

Fu, G., Deming, D., May, E., et al. 2021, AJ, 162, 271, doi: [10.3847/1538-3881/ac3008](https://doi.org/10.3847/1538-3881/ac3008)

Fu, G., Sing, D. K., Lothringer, J. D., et al. 2022a, arXiv e-prints, arXiv:2201.02261. <https://arxiv.org/abs/2201.02261>

Fu, G., Sing, D. K., Deming, D., et al. 2022b, AJ, 163, 190, doi: [10.3847/1538-3881/ac58fc](https://doi.org/10.3847/1538-3881/ac58fc)

Gandhi, S., & Madhusudhan, N. 2019, MNRAS, 485, 5817, doi: [10.1093/mnras/stz751](https://doi.org/10.1093/mnras/stz751)

Gaudi, B. S., Stassun, K. G., Collins, K. A., et al. 2017, Nature, 546, 514, doi: [10.1038/nature22392](https://doi.org/10.1038/nature22392)

Gibson, N. P., Nugroho, S. K., Lothringer, J., Maguire, C., & Sing, D. K. 2022, MNRAS, 512, 4618, doi: [10.1093/mnras/stac091](https://doi.org/10.1093/mnras/stac091)

Gillon, M., Anderson, D. R., Collier-Cameron, A., et al. 2014, A&A, 562, L3, doi: [10.1051/0004-6361/201323014](https://doi.org/10.1051/0004-6361/201323014)

Gray, D. F. 2005, The Observation and Analysis of Stellar Photospheres, 3rd edn. (Cambridge: Cambridge University Press)

Gressier, A., Lecavelier des Etangs, A., Sing, D. K., et al. 2023, A&A, 672, A34, doi: [10.1051/0004-6361/202244429](https://doi.org/10.1051/0004-6361/202244429)

Guillot, T. 2010, A&A, 520, A27, doi: [10.1051/0004-6361/200913396](https://doi.org/10.1051/0004-6361/200913396)

Guilluy, G., Sozzetti, A., Brogi, M., et al. 2019, A&A, 625, A107, doi: [10.1051/0004-6361/201834615](https://doi.org/10.1051/0004-6361/201834615)

Hartman, J. D., Bakos, G. Á., Béky, B., et al. 2012, AJ, 144, 139, doi: [10.1088/0004-6256/144/5/139](https://doi.org/10.1088/0004-6256/144/5/139)

Haynes, K., Mandell, A. M., Madhusudhan, N., Deming, D., & Knutson, H. 2015, ApJ, 806, 146, doi: [10.1088/0004-637X/806/2/146](https://doi.org/10.1088/0004-637X/806/2/146)

Hellier, C., Anderson, D. R., Collier Cameron, A., et al. 2014, MNRAS, 440, 1982, doi: [10.1093/mnras/stu410](https://doi.org/10.1093/mnras/stu410)

Hellier, C., Anderson, D. R., Barkaoui, K., et al. 2019, MNRAS, 490, 1479, doi: [10.1093/mnras/stz2713](https://doi.org/10.1093/mnras/stz2713)

Herman, M. K., de Mooij, E. J. W., Jayawardhana, R., & Brogi, M. 2020, AJ, 160, 93, doi: [10.3847/1538-3881/ab9e77](https://doi.org/10.3847/1538-3881/ab9e77)

Hoeijmakers, H. J., Kitzmann, D., Morris, B. M., et al. 2024, A&A, 685, A139, doi: [10.1051/0004-6361/202244968](https://doi.org/10.1051/0004-6361/202244968)

Hooton, M. J., Hoyer, S., Kitzmann, D., et al. 2022, A&A, 658, A75, doi: [10.1051/0004-6361/202141645](https://doi.org/10.1051/0004-6361/202141645)

Hord, B. J., Kempton, E. M. R., Mikal-Evans, T., et al. 2023, arXiv e-prints, arXiv:2308.09617, doi: [10.48550/arXiv.2308.09617](https://doi.org/10.48550/arXiv.2308.09617)

Ilyin, I. V. 2000, PhD thesis, Astronomy Division Department of Physical Sciences P.O.Box 3000 FIN-90014 University of Oulu Finland

Johnson, M. C., Wang, J., Pai Asnodkar, A., et al. 2023, AJ, 165, 157, doi: [10.3847/1538-3881/acb7e2](https://doi.org/10.3847/1538-3881/acb7e2)

Kasper, D., Bean, J. L., Line, M. R., et al. 2023, AJ, 165, 7, doi: [10.3847/1538-3881/ac9f40](https://doi.org/10.3847/1538-3881/ac9f40)

Kausch, W., Noll, S., Smette, A., et al. 2015, A&A, 576, A78, doi: [10.1051/0004-6361/201423909](https://doi.org/10.1051/0004-6361/201423909)

Kitzmann, D., Stock, J. W., & Patzer, A. B. C. 2024, MNRAS, 527, 7263, doi: [10.1093/mnras/stad3515](https://doi.org/10.1093/mnras/stad3515)

Kochukhov, O., Makaganiuk, V., & Piskunov, N. 2010, A&A, 524, A5, doi: [10.1051/0004-6361/201015429](https://doi.org/10.1051/0004-6361/201015429)

Lendl, M., Csizmadia, S., Deline, A., et al. 2020, A&A, 643, A94, doi: [10.1051/0004-6361/202038677](https://doi.org/10.1051/0004-6361/202038677)

Lothringer, J. D., Barman, T., & Koskinen, T. 2018, ApJ, 866, 27, doi: [10.3847/1538-4357/aadd9e](https://doi.org/10.3847/1538-4357/aadd9e)

Lund, M. B., Rodriguez, J. E., Zhou, G., et al. 2017, AJ, 154, 194, doi: [10.3847/1538-3881/aa8f95](https://doi.org/10.3847/1538-3881/aa8f95)

Mancini, L., Southworth, J., Mollière, P., et al. 2019, MNRAS, 485, 5168, doi: [10.1093/mnras/stz661](https://doi.org/10.1093/mnras/stz661)

Mansfield, M., Bean, J. L., Line, M. R., et al. 2018, AJ, 156, 10, doi: [10.3847/1538-3881/aac497](https://doi.org/10.3847/1538-3881/aac497)

McKemmish, L. K., Masseron, T., Hoeijmakers, H. J., et al. 2019, MNRAS, 488, 2836, doi: [10.1093/mnras/stz1818](https://doi.org/10.1093/mnras/stz1818)

McKemmish, L. K., Yurchenko, S. N., & Tennyson, J. 2016, MNRAS, 463, 771, doi: [10.1093/mnras/stw1969](https://doi.org/10.1093/mnras/stw1969)

Mikal-Evans, T., Sing, D. K., Goyal, J. M., et al. 2019, MNRAS, 488, 2222, doi: [10.1093/mnras/stz1753](https://doi.org/10.1093/mnras/stz1753)

Mollière, P., Wardenier, J. P., van Boekel, R., et al. 2019, A&A, 627, A67, doi: [10.1051/0004-6361/201935470](https://doi.org/10.1051/0004-6361/201935470)

Nikolov, N., Sing, D. K., Goyal, J., et al. 2018, MNRAS, 474, 1705, doi: [10.1093/mnras/stx2865](https://doi.org/10.1093/mnras/stx2865)

Nugroho, S. K., Gibson, N. P., de Mooij, E. J. W., et al. 2020, ApJL, 898, L31, doi: [10.3847/2041-8213/aba4b6](https://doi.org/10.3847/2041-8213/aba4b6)

Nugroho, S. K., Kawahara, H., Masuda, K., et al. 2017, AJ, 154, 221, doi: [10.3847/1538-3881/aa9433](https://doi.org/10.3847/1538-3881/aa9433)

Pai Asnodkar, A., Wang, J., Gaudi, B. S., et al. 2022, AJ, 163, 40, doi: [10.3847/1538-3881/ac32c7](https://doi.org/10.3847/1538-3881/ac32c7)

Parmentier, V., Line, M. R., Bean, J. L., et al. 2018, A&A, 617, A110, doi: [10.1051/0004-6361/201833059](https://doi.org/10.1051/0004-6361/201833059)

Pelletier, S., Benneke, B., Darveau-Bernier, A., et al. 2021, AJ, 162, 73, doi: [10.3847/1538-3881/ac0428](https://doi.org/10.3847/1538-3881/ac0428)

Petz, S., Johnson, M. C., Asnodkar, A. P., et al. 2024, MNRAS, 527, 7079, doi: [10.1093/mnras/stad3481](https://doi.org/10.1093/mnras/stad3481)

Pino, L., D'ésert, J.-M., Brogi, M., et al. 2020, The Astrophysical Journal Letters, 894, L27, doi: [10.3847/2041-8213/ab8c44](https://doi.org/10.3847/2041-8213/ab8c44)

Pluriel, W., Whiteford, N., Edwards, B., et al. 2020, AJ, 160, 112, doi: [10.3847/1538-3881/aba000](https://doi.org/10.3847/1538-3881/aba000)

Prinoth, B., Hoeijmakers, H. J., Kitzmann, D., et al. 2022, Nature Astronomy, 6, 449, doi: [10.1038/s41550-021-01581-z](https://doi.org/10.1038/s41550-021-01581-z)

Ramkumar, S., Gibson, N. P., Nugroho, S. K., Maguire, C., & Fortune, M. 2023, Monthly Notices of the Royal Astronomical Society, 525, 2985, doi: [10.1093/mnras/stad2476](https://doi.org/10.1093/mnras/stad2476)

Rasmussen, K. C., Brogi, M., Rahman, F., et al. 2022, AJ, 164, 35, doi: [10.3847/1538-3881/ac6bfa](https://doi.org/10.3847/1538-3881/ac6bfa)

Rathcke, A. D., Buchhave, L. A., Mendonça, J. M., et al. 2023, MNRAS, 522, 582, doi: [10.1093/mnras/stad1010](https://doi.org/10.1093/mnras/stad1010)

Ricker, G. R., Winn, J. N., Vanderspek, R., et al. 2015, Journal of Astronomical Telescopes, Instruments, and Systems, 1, 014003, doi: [10.1117/1.JATIS.1.1.014003](https://doi.org/10.1117/1.JATIS.1.1.014003)

Rivlin, T., Lodi, L., Yurchenko, S. N., Tennyson, J., & Le Roy, R. J. 2015, Monthly Notices of the Royal Astronomical Society, 451, 634, doi: [10.1093/mnras/stv979](https://doi.org/10.1093/mnras/stv979)

Rosenthal, L. J., Fulton, B. J., Hirsch, L. A., et al. 2021, ApJS, 255, 8, doi: [10.3847/1538-4365/abe23c](https://doi.org/10.3847/1538-4365/abe23c)

Roth, A., Parmentier, V., & Hammond, M. 2024, MNRAS, 531, 1056, doi: [10.1093/mnras/stae984](https://doi.org/10.1093/mnras/stae984)

Scandariato, G., Borsa, F., Bonomo, A. S., et al. 2023, A&A, 674, A58, doi: [10.1051/0004-6361/202245539](https://doi.org/10.1051/0004-6361/202245539)

Schlawin, E., Mukherjee, S., Ohno, K., et al. 2024, arXiv e-prints, arXiv:2406.15543, doi: [10.48550/arXiv.2406.15543](https://doi.org/10.48550/arXiv.2406.15543)

Serindag, D. B., Nugroho, S. K., Mollière, P., et al. 2021, A&A, 645, A90, doi: [10.1051/0004-6361/202039135](https://doi.org/10.1051/0004-6361/202039135)

Siverd, R. J., Beatty, T. G., Pepper, J., et al. 2012, ApJ, 761, 123, doi: [10.1088/0004-637X/761/2/123](https://doi.org/10.1088/0004-637X/761/2/123)

Smette, A., Sana, H., Noll, S., et al. 2015, A&A, 576, A77, doi: [10.1051/0004-6361/201423932](https://doi.org/10.1051/0004-6361/201423932)

Smith, P., Line, M., Bean, J., et al. 2023, arXiv e-prints, arXiv:2312.13069. <https://arxiv.org/abs/2312.13069>

Stangret, M., Pallé, E., Casasayas-Barris, N., et al. 2021, A&A, 654, A73, doi: [10.1051/0004-6361/202040100](https://doi.org/10.1051/0004-6361/202040100)

Stassun, K. G., Collins, K. A., & Gaudi, B. S. 2017, AJ, 153, 136, doi: [10.3847/1538-3881/aa5df3](https://doi.org/10.3847/1538-3881/aa5df3)

Stock, J. W., Kitzmann, D., & Patzer, A. B. C. 2022, MNRAS, 517, 4070, doi: [10.1093/mnras/stac2623](https://doi.org/10.1093/mnras/stac2623)

Stock, J. W., Kitzmann, D., Patzer, A. B. C., & Sedlmayr, E. 2018, MNRAS, 479, 865, doi: [10.1093/mnras/sty1531](https://doi.org/10.1093/mnras/sty1531)

Strassmeier, K. G., Ilyin, I., & Steffen, M. 2018, A&A, 612, A44, doi: [10.1051/0004-6361/201731631](https://doi.org/10.1051/0004-6361/201731631)

Strassmeier, K. G., Ilyin, I., Järvinen, A., et al. 2015, Astronomische Nachrichten, 336, 324, doi: [10.1002/asna.201512172](https://doi.org/10.1002/asna.201512172)

Talens, G. J. J., Spronck, J. F. P., Lesage, A. L., et al. 2017, A&A, 601, A11, doi: [10.1051/0004-6361/201630319](https://doi.org/10.1051/0004-6361/201630319)

Tamuz, O., Mazeh, T., & Zucker, S. 2005, MNRAS, 356, 1466, doi: [10.1111/j.1365-2966.2004.08585.x](https://doi.org/10.1111/j.1365-2966.2004.08585.x)

Valenti, J. A., & Piskunov, N. 1996, A&AS, 118, 595

—. 2012, SME: Spectroscopy Made Easy, Astrophysics Source Code Library, record ascl:1202.013. <http://ascl.net/1202.013>

Wang, J., Prato, L., & Mawet, D. 2017, ApJ, 838, 35, doi: [10.3847/1538-4357/aa6345](https://doi.org/10.3847/1538-4357/aa6345)

Wang, Y.-H., Wang, S., Hinse, T. C., et al. 2019, AJ, 157, 82, doi: [10.3847/1538-3881/aaf6b6](https://doi.org/10.3847/1538-3881/aaf6b6)

Watanabe, N., Narita, N., & Hori, Y. 2024, arXiv e-prints, arXiv:2402.17325, doi: [10.48550/arXiv.2402.17325](https://doi.org/10.48550/arXiv.2402.17325)

Wende, S., Reiners, A., Seifahrt, A., & Bernath, P. F. 2010, A&A, 523, A58, doi: [10.1051/0004-6361/201015220](https://doi.org/10.1051/0004-6361/201015220)

West, R. G., Hellier, C., Almenara, J. M., et al. 2016, A&A, 585, A126, doi: [10.1051/0004-6361/201527276](https://doi.org/10.1051/0004-6361/201527276)

Wong, I., Knutson, H. A., Kataria, T., et al. 2016, ApJ, 823, 122, doi: [10.3847/0004-637X/823/2/122](https://doi.org/10.3847/0004-637X/823/2/122)

Yadin, B., Veness, T., Conti, P., et al. 2012, arXiv: Solar and Stellar Astrophysics

Yan, F., Pallé, E., Reiners, A., et al. 2020, A&A, 640, L5, doi: [10.1051/0004-6361/202038294](https://doi.org/10.1051/0004-6361/202038294)

—. 2022, A&A, 661, L6, doi: [10.1051/0004-6361/202243503](https://doi.org/10.1051/0004-6361/202243503)

Yan, F., Nortmann, L., Reiners, A., et al. 2023, A&A, 672, A107, doi: [10.1051/0004-6361/202245371](https://doi.org/10.1051/0004-6361/202245371)